Supertough Thermoplastic Elastomers of Polystyrene and Polyisoprene via the Pom-Pom Topology

Valerian Hirschberg,* Max G. Schußmann, Marie-Christin Röpert, Nico Dingenouts, Simon Buchheiser, Hermann Nirschl, Jonathan Berson, and Manfred Wilhelm

ABSTRACT: High-performance polystyrene (PS)−polyisoprene (PI) low-disperse thermoplastic elastomers with a well-defined pom-pom topology are synthesized via anionic polymerization techniques, where two stars with each about 13 PS-*b*-PI arms are connected by a linear PS chain, with PI forming the inner core of the star. Samples with 70, 50, 30, and 10 vol % total PS content were prepared. First, a PI-*b*-PS-*b*-PI triblock copolymer (short PI block, $M_{w,PI}$ = 5 kg mol^{-1}, $M_{w,PS}$ = 100 kg mol^{-1}) was synthesized via anionic polymerization; second, the PI blocks were functionalized via epoxidation; and third, PS-*b*-PI anions were grafted onto the outer PI parts of the backbone, forming the pom-pom topology. Mechanical tensile testing at room temperature found extreme strain hardening, resulting in very high true strain at break and stress at break (ultimate tensile stress, UTS). For the pom-pom with 30 vol % PS σ_{UTS} = 30 MPa and ε_b = 1200% and with 10 vol % PS σ_{UTS} = 20 MPa and ε_b = 1500% could be reached. The synthesized model pom-poms match the mechanical performance of the best PS−PI model systems reported in the literature, e.g., UTS of ca. σ_{UTS} = 20 MPa for linear and branched PS−PI model systems, and the pom-pom with 30 vol % PS outperforms the UTS reported in the literature by nearly 50%.

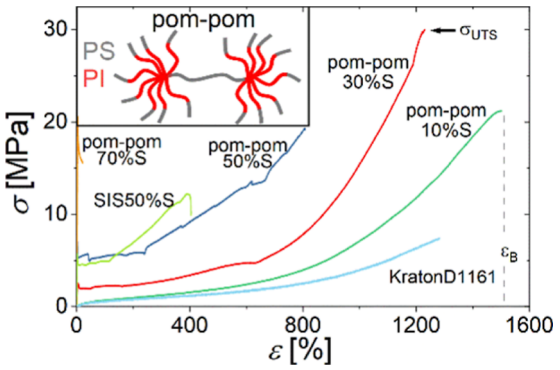

1. INTRODUCTION

Thermoplastic elastomers (TPEs) combine the mechanical behavior of chemically cross-linked rubbers—such as softness, elasticity, flexibility, high elongation at break, and fatigue resilience—with the processability of thermoplastics polymers. The processability and recyclability offer a huge advantage of TPE over classical, chemically cross-linked rubbers, which often also contain further additives, e.g., fillers to increase the mechanical strength.[1] To generate the mechanical strength of TPE, chemical cross-linking is replaced by physical cross-linking via phase separation of a block built of monomer A and built of monomer B, with one T_g below and one above the application temperature, resulting in a combination of soft and hard mechanical properties.[2] Block copolymers tend to phase-separate due to a thermodynamic process driven by the repulsion of unequal segmental contacts, forming micro-domains highly enriched in blocks of the same kind of monomer. Although other mean field theories may provide a more complete description of this phase-separation behavior,[3,4] the simpler Flory−Huggins theory is widely used to gain a basic understanding and predict the phase separation via the Gibbs free energy ΔG_m[5] of polymer chains placed into a lattice. The Gibbs free energy depends on the interactions of the copolymerized monomers, which are described by the monomer−monomer-interaction-based mixing (Flory−Huggins) parameter χ (normalized to kT), the total degree of polymerization N, and the volume fraction of each block $f_{A,B}$. Below the order−disorder transition temperature, T_{ODT}, phase separation occurs, when the product $N\chi$ is above a critical threshold value. This critical threshold value depends on the interacting monomers, the volume fraction of each block, the block order, and the molecular topology (diblock, triblock, star, comb, etc.).[6] Typically, the minimum $N\chi$ for phase separation to occur is at $f_A = f_B = 0.5$ and is, e.g., $N\chi = \sim 10$ for AB diblocks,[7] $N\chi = \sim 13$ for asymmetric triblock copolymer stars $(ABA')_3$ and (miktoarm) stars $A(BA')_3$ (exemption: $f_A/f_B = 0.45$),[8] and $N\chi = 18$ for symmetric ABA triblock copolymers.[9]

Commonly, TPEs are ABA block copolymers, with rigid A blocks outside (e.g., polystyrene, PS) and a soft elastomeric B block (e.g., polyisoprene, PI) in between the A blocks. Both ends of elastomer segment block B need to be linked to glassy domains of block A, locking the elastomer segment into position. Well-known examples of ABA triblocks of polystyrene (S) and polybutadiene (B) or polystyrene and polyisoprene (I)

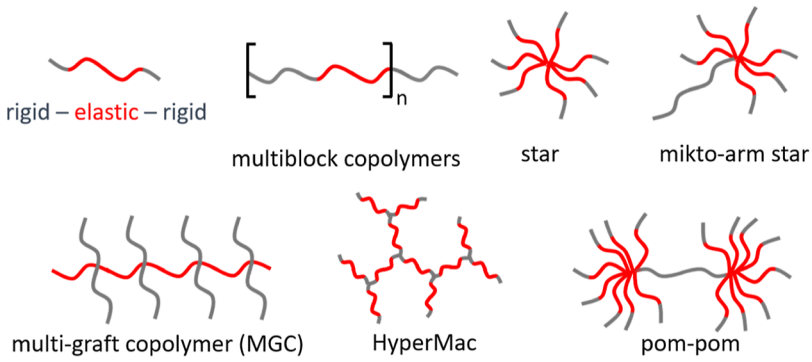

Figure 1. Topology of TPEs: the common ABA triblock, where the rigid block A (gray, e.g., PS) forms the physical cross-linking of the soft/elastomeric block B (red, e.g., PI), a multiblock copolymer, a star, an example of a miktoarm star, the hyperbranched so-called HyperMac architecture, MGCs with an elastic backbone and rigid arms and with a rigid backbone but elastic arms, and the pom-pom topology that is investigated within this article.

are SBS and SIS rubbers, such as commercial Kraton.[2,5] For ABA triblock copolymer TPEs, a continuous B matrix with a spherical or hexagonal cylindrical microstructure of A is targeted; therefore, the maximal volume fraction of the rigid component is limited according to the phase diagram. For PS–PI block copolymers, χ is at room temperature around 0.1,[10] so according to the phase diagrams typically less than 35 vol % of the rigid PS component can be copolymerized to avoid a lamellar structure.

To overcome limitations between the rigid/elastic volume fraction and the morphology, new topologies besides the classic ABA triblock were introduced in the literature. In addition to multiblock copolymers such as, e.g., ABABA pentablock copolymers[11−14] and linear low disperse SIS with different shapes of the MWD of the first S block,[15−17] asymmetric triblock copolymers (ABA′)[18,19] mainly branched topologies are employed, as schematically shown in Figure 1: stars, branched comb-like multigraft copolymers (MGCs),[20−25] and miktoarm stars.[18,26−28] The pom-pom topology is the subject of this article. A commercial example of a PS–PI copolymer with a star-like topology is, e.g., Styroflex.[29,30]

The mechanical properties of the branched TPEs are highly tunable compared to those of the classic ABA triblocks. PS–PI star-shaped block copolymers were found to increase the stress at break, but decrease the elongation at break, since star polymers have more condensed physical cross-links per unit volume.[31−33] In MGC topologies, such as comb and barbwire[22−24] or the hyperbranched so-called HyperMac from the polycondensation of $\alpha,\omega,\grave{\omega}$-trifunctional SIS triblock macromonomers (see Figure 1)[34−36] structures, the elastic/soft backbone is physically cross-linked via the phase separation of the grafted rigid arms. Comb-like MGC structures were found to highly improve especially the ultimate tensile stress (UTS), the elongation at break, and their elasticity, i.e., reduced plasticity under cyclic loading.[2,22,23] Additionally, the elongation at break and the UTS were found to depend on the topology, e.g., the number of branching points. The inverse topology MGC was also proposed, with a rigid backbone and soft/mobile arms,[37] although no data are available for an MGC with PI grafted onto a PS backbone. Miktoarm (mixed arm) star copolymers are stars with asymmetric arms in terms of molecular weight, chemistry, or topology,[38,39] e.g., with A and BA arms. Motivated by self-consisting field theory, miktoarm stars of PS–PI were developed, which allow to completely uncouple the rigid/elastic volume fraction–morphology relationship.[8,18,26−28] Some miktoarm stars formed even at high volume ratios of PS beyond 90% a lamellar morphology.[28] Furthermore, the number of arms at the conjunction points of miktoarm stars allows for shifting morphology at the same A/B volume fraction, showing for a $PS(PDMS)_2$ and $PS(PDMS)_3$ with 67 vol % PS a hexagonal cylindric and BCC spherical microdomain structure, respectively.[40]

Under uniaxial elongation in the solid state, TPEs typically display either ductile or rubber-/elastomer-like mechanical behavior. Characteristic for ductile behavior is a comparably high Young's/E-modulus (E > 10 MPa), and yielding with a stress maximum, followed by necking and plastic deformation.[41] For rubber/elastomer-like behavior a low modulus, no distinct yielding, and high elasticity, i.e., low plastic deformation even at large strains is characteristic. The microdomain structure and PI content determine whether ductile or elastomeric behavior occurs. Failure of TPEs under elongation ($T < T_{g,hard}$) arises because of the rupture of the glassy domains, which are held together by chain entanglement. To create highly mechanically performing TPEs, strain hardening is of high importance, representing the constraints of molecules to flow under elongation, resulting in a (drastic) stress increase at large strains. Consequently, strain hardening allows the expansion of a material to higher elongations without rupture. In TPEs, strain hardening is commonly induced via phase separation and the physical cross-linking via the PS domains, not via the covalent bonds usually present in classical elastomers.[2] Therefore, also temperature effects are to be expected; a higher difference between the temperature of usage and the glass temperature of rigid domains is favorable.

The objective of this article is to present a simple synthetic route to obtain PS-*b*-PI TPE with a defined pom-pom topology (see Figure 1), where rigid-*b*-soft diblocks with different PS and PI content are grafted onto both ends of a rigid backbone of a fixed, defined M_W, so that four different pom-pom model systems with in total 70, 50 30 and 10 vol % PS are obtained. We then investigate how the pom-pom topology affects the morphology as well as the solid mechanical properties ($T < T_{g,rigid}$) for the different PS and PI volume fractions. This pom-pom-shaped topology combines several important structure–property features. (I) First, the outer block is the rigid PS block, so the PI chains are physically fixed in the PS domains at both ends. (II) Second, a star-like topology is known to

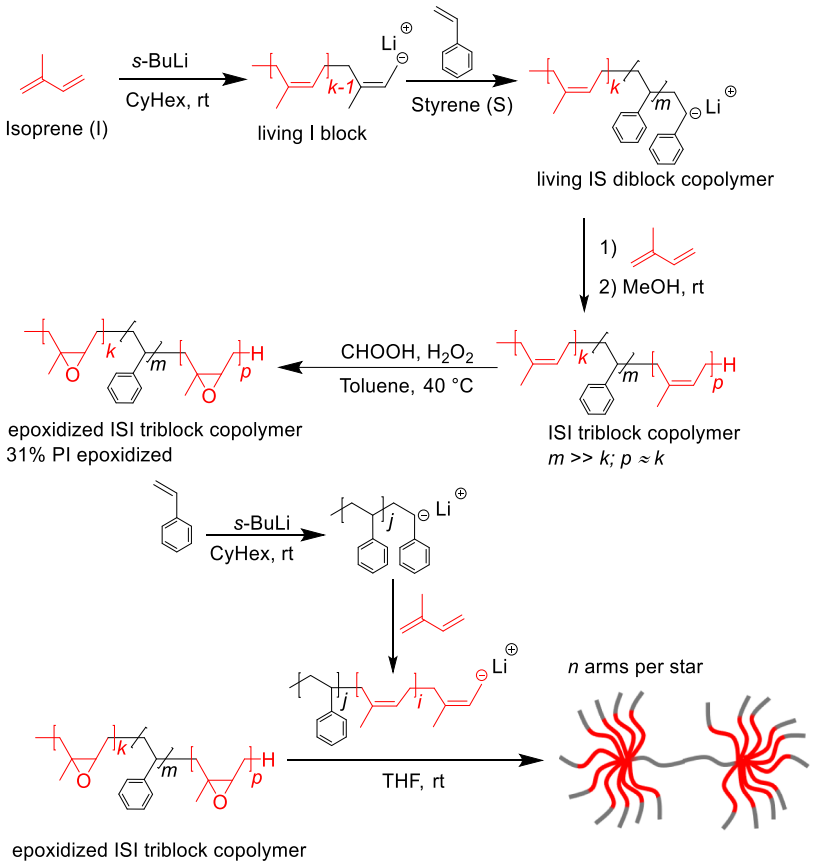

Figure 2. Synthesis of PS−PI pom-poms via a combination of anionic polymerization of an ISI triblock backbone, subsequent epoxidation of the *cis*-1,4 PI for functionalization, and grafting onto, by grafting PS-*b*-PI arms onto a PI-*b*-PS-*b*-PI backbone. The 31% of epoxidized PI was determined via NMR, and the NMR spectrum of the epoxidized backbone is shown in Figure S1 in the Supporting Information.

increase moduli and offers excellent tensile strength. (III) A PS-*b*-PI-*g*-PI-*b*-PS-*b*-PI (SI-*g*-ISI) pom-pom topology can be seen as two connected miktoarm stars with a high number of branches at the connection point, which allows the A/B volume fraction−morphology relationship to be uncoupled. (IV) A high arm number is expected to improve mechanical properties. (V) The PS backbone allows the covalent bridging of the PS domains. If the different PS parts of the pom-pom molecule are in different PS domains, it allows many anchor points of the PI matrix to be connected and consequently transfer forces between them. The results later presented show that for the SI-*g*-ISI pom-poms ultimate stresses beyond the toughest PS−PI block copolymer reported in the literature could be achieved.[18,24,25,31]

2. SYNTHESIS AND MATERIALS

2.1. Materials and Methods. Styrene (99%, extra pure, Sigma-Aldrich) was purified by distillation after stirring one night over calcium hydride (CaH_2, 92%, Fisher Scientific). Then, the monomer was distilled from di-*n*-butyl magnesium (0.5 M, Fisher Scientific) into ampules and degassed afterward by three successive freezing−evacuation−thawing cycles. Isoprene (98%, VWR) was purified by first cooling the monomer in an ice bath and then adding *n*-butyllithium (2.6 M in cyclohexane, Sigma-Aldrich). As soon as the solution turned yellowish, the monomer was distilled into an ampule. The purified monomers were stored under an argon atmosphere at −18 °C until needed. Cyclohexane (99%, Fisher Scientific) was stored over living PS and distilled before use. Tetrahydrofuran (99.5%, Roth), THF, was distilled from CaH_2, stored over sodium/benzophenone, and distilled before synthesis. 1,4-Dioxane (≥99.8%, Fisher Scientific) was distilled to remove the stabilizer. Methanol (>99%, Fisher Scientific) was degassed by three successive freezing−evacuation−thawing cycles. Toluene (>99%, Roth), hydrogen peroxide (H_2O_2, 30 wt %., Acros), formic acid (98%, Roth), and *sec*-butyllithium (*s*-BuLi, 1.4 M in cyclohexane, Aldrich) were used as received. For SEC measurements, SEC grade THF was used (0.025% dibutylhydroxytoluene, BHT, Fisher Scientific); see Supporting Information for more details.

NMR measurements were performed with a Bruker AVANCE III Microbay 400 MHz spectrometer with the samples dissolved in deuterated chloroform (CDCl3, 99.8%, Sigma-Aldrich) and signals were referenced to the solvent peak at δ 7.26 ppm.

Small-angle X-ray scattering was done using a Xeuss 2.0 Q-Xoom, Xenocs SA, Grenoble, France, with a *q*-space from $q = 0.001-4$ nm^{-1}. Atomic force microscopy (AFM) was done in the semicontact mode using a Bruker dimension ICON system, equipped with the following tips: Opus 160AC-NA by Mikromasch with a force constant of 26 N/m. The AFM samples were prepared with spin-coating at 5000 rpm onto bare silica wavers from 0.3 wt % solutions in toluene, yielding films with a thickness of 15 ± 1 nm.

2.2. Synthesis of SI-*g*-ISI Pom-Poms. The SI-*g*-ISI pom-poms were synthesized via a combination of anionic polymerization, functionalization, and grafting onto, as shown in Figure 2, similar to the preparation of PS pom-poms reported in the literature.[42,43] First, an ISI backbone was synthesized via anionic polymerization, where the PI blocks are around 10 mol % of the PS block. Second, the PI blocks were functionalized by epoxidation of the unsaturated double bonds with H_2O_2 and formic acid. Third, living SI anions were grafted onto the epoxidized blocks.

2.2.1. Anionic Polymerization of the Backbone. An ISI backbone was synthesized via living anionic polymerization in dry cyclohexane (200 mL) at room temperature using high-vacuum techniques. The

Table 1. Molecular Parameters of the Synthesized SI-*g*-ISI Pom-Poms with $M_{w,b}$ = 100 kg mol^{-1}, the Linear SIS, and the Commercial TPE KratonD1161[a]

sample	$M_{n,a}$ [kg mol^{-1}]	$f_{PS,a}$ [mol %]	n	$Đ_a$	$M_{n,t}$ [kg mol^{-1}]	$Đ_t$	$f_{PS,t}$ [vol %]	L_0 [nm]	bulk morphology
pom-pom70%S	81.1	66.3	2 × 9	1.06	1550	1.09	70.3	29.9	S/C
pom-pom50%S	120	41.3	2 × 12	1.10	2970	1.40	55.7	43.3	L
pom-pom30%S	106	24.9	2 × 14	1.08	3060	1.29	29.3	29.9	C
pom-pom10%S	117	7.6	2 × 13	1.07	3130	1.34	11.1	27.5	S
SIS70%S					193	1.1	69.6	32.5	S
SIS50%S					170	1.15	44	55.3	L
SIS30%S					202	1.07	29.8	57.1	C
SIS10%S					227	1.09	9.2	34.9	S
KratonD1161					112	1.42	11	33.7	S

[a]The molecular weight of the arms, $M_{n,a}$, the PI mol content of the arms, $f_{PI,a}$, the number of arms, n, the total molecular weight, $M_{W,t}$, the PI volume fraction in the pom-pom, $f_{PI,t}$, investigated with ^{1}H NMR and calculated using densities of PS and PI as ρ_{PS} = 1050 kg/m^3, and ρ_{PI} = 920 kg/m^3, the long-range order distance L_0, determined by SAXS and the morphology (S for a spherical, C for a hexagonal cylindrical, L for a lamellar, and dis for a disordered morphology). The SEC traces of the pom-poms can be found in the Supporting Information. The number of side chains n was quantified by two methods. The first one back-calculates the number of side chains due to the known total molecular weights (MALLS) of both the side chains and the backbone. The second method is based on the ratio of the area under the SEC trace of unreacted side chains to that of the pom-pom product.

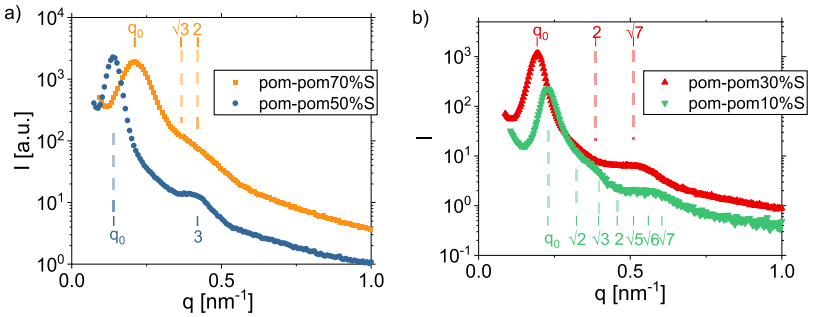

Figure 3. Azimuthally averaged 1D plot of the scattering intensity, i.e., SAXS pattern of the four pom-poms investigated. In (a) for pom-pom70%S, a shoulder at $\sqrt{3}q_0$ can be seen, whereas pom-pom50%S shows a shoulder at $3q_0$, indicating a cylindrical or spherical and symmetric lamellar morphology. For the pom-pom50%S, one could assume a small side structure at roughly $2q_0$ confirming the lamellar morphology and indicating not perfectly equal volumes of the two phases, but very close to 50/50 vol %, please see also the Supporting Information for not assigned peaks. In (b) for the pom-pom30%S, a shoulder between 2 and $\sqrt{7}q_0$ and a small indication at $\sqrt{3}q_0$ (clearly not at $\sqrt{2}q_0$, see Figure S7 in the Supporting Information) can be seen. The most probable structure therefore is a cylindrical morphology (also seen in the literature for MGC). For the pom-pom10%S, a similar shoulder between 2 and $\sqrt{7}q_0$ is present, but below $2q_0$ is an additional structure ranging from $\sqrt{2}q_0$ to $\sqrt{3}q_0$, especially the $\sqrt{2}q_0$ is a clear indication of a spherical morphology.

comonomers were added sequentially to the reaction flask after the complete conversion (sufficient reaction time) of the previous block (V(styrene) = 9.9 mL, V(isoprene) = 0.74 mL for each block, and V(*s*-BuLi) = 0.07 mL). Subsequently, the living anionic chains of the triblock were terminated with degassed methanol and the resulting polymer was precipitated in a large excess of methanol. The resulting backbone had a molecular weight of $M_{w,b} \cong 100$ kg mol^{-1} (total degree of polymerization $P_n \approx 940$). The M_W of the PI blocks at each end of the ISI backbone is $M_{w,PI}$ = 5 kg mol^{-1}, corresponding to approximately 70 isoprene units on each side.

2.2.2. Epoxidation of the PI Blocks. The PI parts of the synthesized ISI backbone (10 g) were epoxidized in toluene (200 mL) at 40 °C with H_2O_2 (1.77 g, 30 wt %) and formic acid (0.75 g) as a catalyst, as described in the literature.[44] Afterward, the epoxidized ISI backbone was freeze-dried out of destabilized dioxane to remove residual amounts of protic compounds, like water.

2.2.3. Anionic Polymerization of the Arms and Grafting Onto. The living anionic SI arms (e.g., for the pom-pom50%S: V(styrene) = 11 mL, V(isoprene) = 14.7 mL for each block, V(*s*-BuLi) = 0.204 mL, m_b = 0.62 g) were synthesized by similar reaction steps as the backbone in cyclohexane (200 mL) and were grafted onto the epoxidized backbone dissolved in THF (100 mL) under argon atmosphere at room temperature to obtain the pom-pom topology, as shown in Figure 2. The resulting SI-*g*-ISI pom-poms were purified by two to three fractionation steps in a cyclohexane/isopropanol mixture for high PI contents and THF/methanol for high PS contents.

As reference samples, four linear SIS samples with PI content similar to that of the pom-poms and a commercial SIS TPE, KratonD1161, were investigated. The SIS were synthesized with sequential anionic polymerization, similar to the synthesis of the backbone and as reported in ref 45. The molecular properties of all investigated systems are listed in Table 1.

2.3. Characterization of Morphology via Small-Angle X-ray Scattering and Atomic Force Microscopy. Microstructural information about the PI and PS microdomains in the solid samples was obtained by small-angle X-ray scattering (SAXS) and AFM. The SAXS pattern in q-space and the AFM images of the investigated pom-pom are shown in Figures 3 and 4. For the pom-pom70%S, the SAXS pattern has a shoulder next to q_0, which is clearly not only $2q_0$ but also something smaller, e.g., $\sqrt{3}q_0$, which is typical for a spherical or hexagonal structure,[46] as also matching the AFM image in Figure 4a, which also indicates a spherical or cylindrical morphology. Additionally, $\sqrt{2}q_0$ is assigned in Figure S7, but it clearly does not indicate another peak. The broad shoulder shows a nonperfect ordering that can be also seen in the AFM Image. The pom-pom50%S shows no significant side-peak below $3q_0$, indicating a symmetric lamellar structure, as also expected from the PS and PI volume fractions. The AFM image in Figure 4b also supports this assumption. The SAXS pattern of pom-pom30%S shows a broad shoulder reaching from $2q_0$ to $\sqrt{7}q_0$, and a very small indication of a peak just

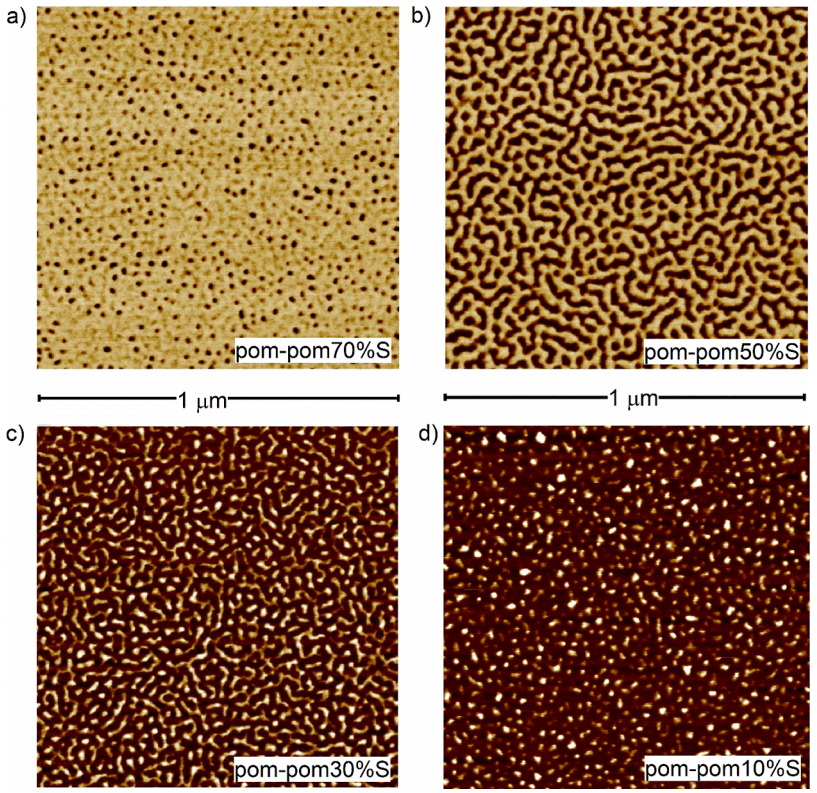

Figure 4. AFM images of the four pom-poms investigated, from (a) to (d) from pom-pom70%S to pom-pom10%S, also indicating the microstructures from the SAXS interpretation. In (a) for the pom-pom70%S, a spherical or cylindrical structure in the above view seems plausible, the spherical seems more favorable, but while there is a clear phase separation, the overall ordering is not pronounced, and in (b) a lamellar morphology with a continuous PS phase for the pom-pom50%S is indicated. In (c) for the pom-pom30%S, a continuous PI phase with PS cylinders can be assumed, with a weak long-range order. A spherical morphology seems a reasonable possibility for the pom-pom10%S in (d) in spite of the fact that the structure in extremely soft material with only 10%S is not perfectly resolved. In all four cases, the morphological interpretation from SAXS and AFM match well.

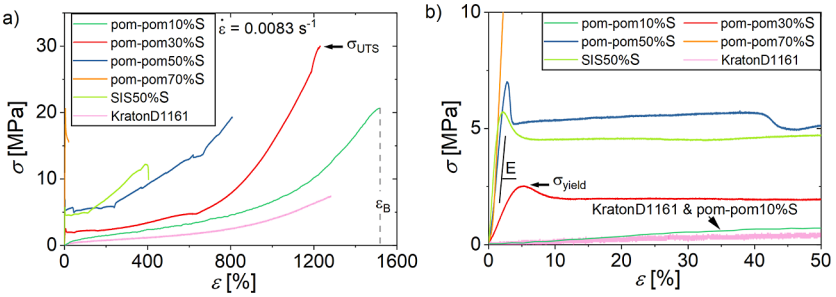

Figure 5. Stress–strain curves in (a) and the zoom-in for the small strain region in (b) of uniaxial tensile testing of the pom-poms, one SIS, and KratonD1161. The true strain at break and the UTS are listed for each specimen in Table 2.

below $2q_0$, at around $\sqrt{3}q_0$ (but not at $\sqrt{2}q_0$, see Figure S7 in the Supporting Information) making it difficult to clearly distinguish the morphology; only the lamellar structure can be clearly ruled out. A similar SAXS pattern has been described in the literature for MGC, showing a weak $2q_0$ peak and a pronounced $\sqrt{7}q_0$ peak combined with a suppressed $\sqrt{3}q_0$ peak, which can be explained by a cylindrical morphology with pronounced minima in the form factor of the cylinder.[20] The AFM in Figure 4c confirms a relatively constant diameter of the cylinders and, therefore, this interpretation. For the pom-pom10%S, a spherical morphology of PS in a PI matrix is indicated by the AFM image and the SAXS pattern, as it shows a similar shoulder from $2q_0$ to $\sqrt{7}q_0$, and also more structure below $2q_0$ roughly from $\sqrt{2}q_0$ to $\sqrt{3}q_0$.

Branched block copolymers are known to have smaller microdomain sizes, as expected for linear triblocks with the same molecular weight.[32] Independent of topology, molecular weight also influences the microdomain size.[45] For a complex but also compact polymer system like the pom-pom topology, due to the branching the total molecular weight is not the only relevant molecular parameter; rather, twice the M_W of the arms is more relevant, as two arms can be seen as a single $(SI)_2$ unit. It can be seen clearly from the long-distance order L_0 (according to Bragg's law, $L_0 = 2\pi/q_0$) values listed that the pom-poms have significantly smaller L_0 values than comparable SIS triblock copolymers with the same M_W as two arms. Similar trends have been found in the literature, e.g., PS–PI stars.[32,33,47]

2.4. Mechanical Characterization. Polymer films were prepared by dissolving 1 g of the polymer in 20 mL of THF and slow evaporation at room temperature and atmosphere pressure of the solvent over about 5 days, followed by drying under vacuum at 60 °C for 2 h. Following the rubber and elastomer testing standard DIN 53504 S3A, specimens with a dumbbell geometry were punched out from solvent-casted films with a gauge length of 10 mm, a width of 4

Table 2. Mechanical Properties *E*-Modulus, ε_b, σ_{UTS}, σ_{yield}, and *U* of the SI-g-ISI Pom-Poms, the Linear SIS and KratonD1161 Investigated

sample	vol % PS	wt % PS	mol % PS	*E*-modulus [MPa]	ε_b [%]	σ_{UTS} [MPa]	σ_{yield} [MPa]	*U* [MJ/m^3]
pom-pom10%S	11.1	14.5	10	1.26 ± 0.18	1519 ± 31	20.3 ± 0.6	0.48 ± 0.07	95.1 ± 7.2
pom-pom30%S	29.3	36	26.9	38 ± 3.5	1191 ± 56	29.2 ± 0.8	3.2 ± 0.33	103 ± 8.3
pom-pom50%S	45.7	53.3	42.8	207 ± 17	752 ± 50	21 ± 0.6	7.0 ± 0.45	80.3 ± 7.6
pom-pom70%S	70.3	86.3	67.7	623 ± 30	20 ± 2	20.1 ± 0.7	20.5 ± 2.1	3.1 ± 0.2
SIS70%S	69.6	75.8	66.9	435 ± 21	42 ± 3.6	16.1 ± 0.6	15.7 ± 1.2	6.5 ± 5.5
SIS50%S	44	51.7	41.2	140 ± 8.3	382 ± 19	11.8 ± 0.4	5.6 ± 0.37	30.4 ± 2.4
SIS30%S	28.8	35.5	26.4	2.6 ± 0.15	1016 ± 42	14.1 ± 0.6	0.5 ± 0.04	58.0 ± 6.1
SIS10%S	11.3	14.5	10	0.25 ± 0.01	1243 ± 66	6.1 ± 0.3	0.3 ± 0.01	22.8 ± 1.7
KratonD1161	11	14.4	9.9	0.28 ± 0.02	1278 ± 58	7.6 ± 0.2	0.28 ± 0.03	31.2 ± 2.1

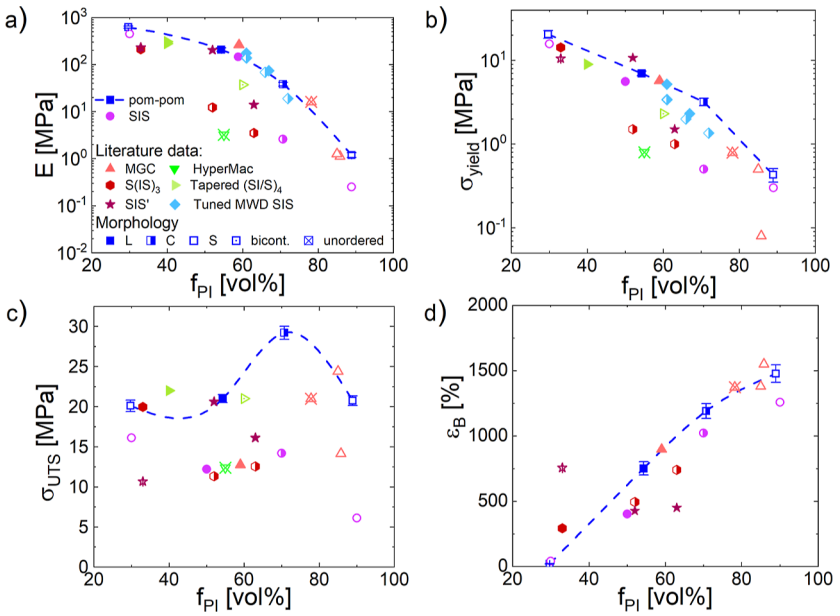

Figure 6. (a) Young's modulus, (b) yield stress, (c) UTS, and (d) true strain/elongation at break of the investigated pom-poms as well as of selected PS−PI TPEs with different complex topologies and morphologies as reported in the literature: MGC ($\dot{\varepsilon}$ = 0.0125 s^{-1};[24] $\dot{\varepsilon}$ = 0.0125 s^{-1};[23] and $\dot{\varepsilon}$ = 0.025 s^{-1}[25]), miktoarm stars ($\dot{\varepsilon}$ = 0.012 s^{-1}),[18] asymmetric triblocks ($\dot{\varepsilon}$ = 0.012 s^{-1}),[18] linear low disperse SIS with different shapes of the MWD of the first S block ($\dot{\varepsilon}$ = 0.016 s^{-1}),[15] PS−PI tapered stars ($\dot{\varepsilon}$ = 0.0038 s^{-1}),[31] and a PS−PI HyperMac ($\dot{\varepsilon}$ = 0.01 s^{-1}).[36] A closed symbol refers to a lamellar, a half open to a hexagonal cylindric, an open with a dot to a bicontinuous, an open symbol to a spherical, and an open crossed symbol to an unordered morphology. In (d), elongation at break data was excluded, if either only engineering strains are reported, or it is not clear whether true or engineering strain is shown.

mm, and a thickness of around 0.25 ± 0.01 mm. Uniaxial and cyclic tensile testing were performed on a universal testing machine Inspect Table 10 from Hegewald and Peschke (Nossen, Germany), equipped with a 1.5 kN force transducer at room temperature. The calibration of the force transducer below 1 N was verified manually with 50 and 10 g weights to ensure reproducible and accurate results. From the stress−strain curve, Young's modulus (*E*-modulus), the stress at yield, σ_y, the UTS, σ_{UTS}, and the elongation at break, ε_b, were obtained. The tests were performed at room temperature with a cross-head speed of 5 mm min^{-1}, resulting in a starting strain rate of $\dot{\varepsilon}$ = 0.0083 s^{-1}. The crosshead strain ε_c was determined from the crosshead (motor) movement and the true strain ε was determined via optical image analysis.

3. RESULTS

3.1. Uniaxial Tensile Testing. To quantify the impact of topology on the mechanical properties, the stress−strain curves of the SI-*g*-ISI pom-pom TPEs were measured, as shown in Figure 5a and in the zoom-in at small strains in (b). From the stress−strain curves, two distinct mechanical behaviors can be observed: ductile behavior of the pom-pom70%S, 50%S, and 30%S, and typical rubber-like behavior for the pom-pom10%S, i.e., without a stress overshoot due to yielding. For the pom-pom70%S, 50%S, and 30%S, at small strains (ε < 2%), the stress−strain curve, i.e., $\sigma(\varepsilon)$, is a straight line, where Young's modulus can be calculated, with *E* > 10 MPa. At larger strains, $\sigma(\varepsilon)$ becomes nonlinear, and the materials yield. At ε larger than yield, plastic deformation occurs, resulting in necking and constant stress. At higher strains (e.g., ε = 250% for pom-pom50%S and ε = 700% for pom-pom30%S), necking is followed by strain hardening before rupture, resulting in an extreme stress increase of a factor of 4 (pom-pom50%S) and 6 (pom-pom30%S) up to about 20 and 30 MPa, respectively.

In contrast to the pom-poms with 70, 50, and 30 vol % PS, the pom-pom10%S does not show ductile behavior with a stress maximum at yielding but rather typical rubber-like behavior (see Figure 5b) because of the low PS content of 10 vol %. Young's modulus of 1.21 MPa is in the typical range for an unfilled rubber (about 1 MPa), and no yielding occurs at low strains. Instead, yielding is rather assumed as the end of the linear regime. Strain hardening can also be observed

starting from about ε = 700% strain, with a drastic stress increase from σ = 3 MPa of about a factor of 7 up to σ = 20.6 MPa at ε = 1500%.

The curves for SIS50%S and the commercial KratonD1161 are shown as examples, and the tensile curves of the other SIS70%S, 30%S, and 10%S are given in the Supporting Information. The commercial sample KratonD1161 as a reference shows similar behavior at small strains and an elongation at break as the pom-pom10%S, but much less strain hardening. Failure occurs for the KratonD1161 sample at a stress of only σ_{UTS} = 7.6 MPa. This is also the case for the SIS50%S and the pom-pom50%S, resulting in a lower UTS and elongation at the break by about a factor of 1.8 and 2, respectively. The mechanical parameters of the other SIS are listed in Table 2. Furthermore, the energy U needed to break a material is calculated from the integral of the stress over the strain from a zero elongation at the beginning of the test until the elongation at break and is listed in Table 2, revealing clearly a significant increase by over a factor of 2 of the pom-pom shaped PS−PI compared to the linear SIS triblocks and the KratonD1161.

The stress at yield, the UTS, and the strain at break of the SI-g-ISI pom-pom were extracted from the uniaxial stress−strain curves as characteristic mechanical parameters and plotted in Figure 6 as a function of the PI content. The morphology of each sample is indicated by the open/closed symbols, closed symbols for a lamellar morphology, half open for a cylindrical, open for a spherical, open with a dot for a bicontinuous and open crossed for an unordered morphology. For comparison, literature data for MGC,[23−25] miktoarm stars,[18] tapered $(SI)_n$ diblock stars,[31] asymmetric SIS′ triblocks,[18] HyperMacs,[34−36] linear low disperse SIS with different shapes of the MWD of the first S block,[15,16] and commercial KratonD1161 were added. The employed crosshead speeds are given in the figure caption. The dashed blue line is a guide for the eyes following the pom-pom values. The comparison with the literature data reflects the influence of molecular topology and the resulting morphology on these mechanical parameters.

As shown in Figure 6a, Young's modulus decreases as expected with increasing PI fraction and follows for the investigated pom-pom70%S, 50%S, and 30%S a power law correlation, before E drops drastically for pom-pom10%S. Compared with literature data, the pom-poms have high moduli and follow the same trend as the majority of the linear as well as branched model systems. The rapid Young's modulus decreases beyond 70 vol % PI can be related to the change from ductile to rubber-like behavior, resulting in drastically reduced Young's modulus. Moreover, some topologies such as the miktoarm star $S(IS')_3$,[18] asymmetric triblock SIS′,[18] or HyperMac[36] allow access to mechanical rubber-like behavior at a lower PI content, resulting in significantly lower Young's moduli. Compared with pom-poms, especially stars are of interest, e.g., the partly tapered triblock copolymer star $(SI/S)_4$[11] with a ductile stress−strain curve has a reduced Young's modulus by about a factor of 4, compared with the dashed blue line of the pom-pom topologies.

Similar to Young's modulus, the yield stress decreases with increasing PI content, as shown in Figure 6b. Again, a substantial reduction can be found between the ductile type TPE and the rubber-like pom-pom10%S, where yielding is defined in literature as the onset of nonlinear stress−strain behavior. Compared with other topologies, the pom-pom topology presented here offers high yield stresses and clearly outperforms especially star and miktoarm star systems. This can be explained like for the Young's modulus, by the ductile type behavior even of pom-pom30%S, whereas, e.g., miktoarm stars with 50 and 40 vol % PS start to behave rather rubber-like with low Young's moduli and yielding at low stresses.

The UTS is of high importance, representing a measure of the maximum load that a material can withstand. The UTS is plotted in Figure 6c as a function of the PI content for the pom-poms and literature data. For the four pom-poms even at only 10 vol % PS, an UTS of $\sigma_{UTS} \geq 20$ MPa can be measured, with a maximum value for the pom-pom30%S of about σ_{UTS} = 30 MPa. For pom-pom70%S, the UTS equals the yield stress, whereas for pom-pom50%S−10%S it equals the stress at break since the material shows strong strain hardening as shown in Figure 5. The commercial KratonD1161 with about 10 vol % PS and the SIS10%S both have a UTS of only $\sigma_{UTS} \approx 7$ MPa, which is lower by about a factor of 3 than for the pom-pom10%S with $\sigma_{UTS} \approx 20$ MPa. The comparison of the UTS and of the elongation at break with literature data on linear SIS and other complex model systems needs to be done carefully, since the measurement conditions and protocols (e.g., $\dot{\varepsilon}$) highly influence stress and strain at break. For example, the UTS typically increases with an increasing strain rate. The UTS of TPE in literature is typically in the range of 10 to 15 MPa at $\dot{\varepsilon}$ = 0.0038 to 0.025 s^{-1}, with a few exceptional topologies, reaching the benchmark of round 20 MPa such as miktoarm and tapered stars and optimized multi graft copolymers. Consequently, the four pom-poms also match this σ_{UTS} = 20 MPa limit and the pom-pom30%S stands out with an UTS of about σ_{UTS} = 30 MPa. The σ_{UTS} = 30 MPa are nearly 50% higher than the 20 MPa benchmark and over more than 5 MPa higher than the highest so far reported σ_{UTS} in the literature for PS−PI systems (to the best of our knowledge). Such a high UTS is especially remarkable, as (I) for any material property there are absolute limits, which cannot simply be extended, and (II) the drastic strain hardening must be the result of the topology and the morphology, underlining the influence of topology and the importance to introduce strain hardening for TPE via well-chosen molecular design.

As shown in Figure 5, the elongation at the break of the pom-pom topologies investigated increases as a function of the PI content (Figure 6d). Pom-pom70%S has an elongation at break of about ε_b = 20%, which is very low compared with literature data of complex topologies with a similar PI content[18] and in the range of a linear SIS. From SAXS analysis, a cylindrical microdomain structure is indicated, so the combination of PI cylinders in a PS matrix in combination with the pom-pom topology seems to result in poor elongation at break. For the other pom-poms, with a continuous PI domain, the extreme strain hardening allows high elongations at the break. For pom-pom30%S and pom-pom10%S, strain hardening accounts for nearly half of the complete stress−strain curve. Compared with literature data and linear SIS, the pom-poms have high elongations at break, and the dashed blue line in Figure 6d seems to well describe the maximum elongation at break that can be optimized by topology.

Comparing the influence of the topology and the morphology on the stress−strain properties of the TPE with pom-pom topology with literature model systems, it is evident that especially the pom-pom with 50, 30, and 10 vol % PS perform in the benchmark range of Young's modulus, yield

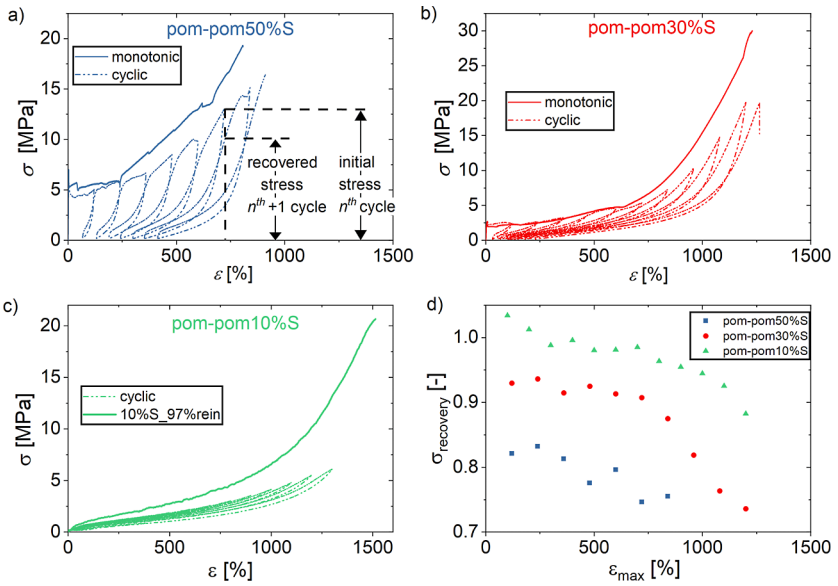

Figure 7. Cyclic engineering stress—true strain curves of pom-pom (a) 50%S, (b) 30%S, and (c) 10%S as well as (d) the stress recovery as a function of the maximum strain for the three pom-poms.

stress, UTS, and elongation at break. Especially the pom-pom30%S outperforms literature systems of PS−PI TPE in terms of UTS with σ_{UTS} = 30 MPa by about 5 to 10 MPa higher values. The massive strain hardening also compared with star or miktoarm star systems could be attributed to the following: (I) the PI blocks are locked in position at both ends in a PS domain. (II) A rigid backbone is employed, locked in a rigid PS domain. (III) The number of arms is known to increase the stress at break for MGC. The here investigated pom-pom model systems have high branching numbers with about 13 ± 1 arms per each of the two stars/branching points. (IV) A high bridging vs looping ratio of the backbone chains[45] can be expected due to the combination of topology and morphology, improving mechanical properties.

3.2. Cyclic Tensile Testing. Step cyclic tensile tests were conducted to investigate plastic deformation and stress recovery after multiple loading. Therefore, the specimens were strained in each *n*th cycle to the *n*th multiple of a strain of 100% ($n \times 100\%$, i.e., 100% in the first cycle, 200% in the second cycle, etc.), followed by unloading to a zero stress at room temperature. Figure 7 shows the engineering stress as a function of the strain for the pom-pom50%S (a), 30%S (b), and 10%S (c) during monotonic and cyclic loading at a crosshead speed of the tensile machine of 5 mm/min. Figure 7a−c shows that during each cycle a plastic strain remains, but high stress recovery occurs. To obtain stress recovery, the stress in the $n + 1$ cycle at the strain peak of the *n*th cycle is normalized to the stress at the *n*th strain peak, as shown schematically in Figure 7a. During cyclic loading for pom-pom50%S and pom-pom30%S, even higher strains than their elongation at break are accessible during monotonic loading, but with lower stress maxima at high strains as for the monotonic test. The cyclic strain softening is most extreme for pom-pom10%S, where the effect of strain hardening nearly totally disappears. This phenomenon is reported in the literature and attributed to the slow pull-out of the PS chains out of their domain, decreasing the hardening effect of the physical cross-linking of the PS blocks.[18] For the pom-pom30% S in cyclic tests, a maximum stress of 19.7 MPa is measured after the 12th cycle, which is still in the maximum range that TPEs with other topologies can reach in uniaxial tensile tests. Furthermore, for pom-pom10%S, after cyclic loadings to 1200 and 1300%, residual strains, i.e., plastic deformations of about 60 and 80%, remain. In literature reports for an MGC under cyclic deformation, a plastic deformation of about 45% remained after 4 cycles with up to ε = 1200%,[24] which is in the same range as the pom-pom10%S. Moreover, plastic deformation is a rate and time-dependent process, so the number of cycles the material is strained previously has a huge impact on the remaining plastic deformation.

The recovery stress after each cycle is plotted in Figure 7d, revealing around 80% stress recovery for the pom-pom50%S, of over 90% for the pom-pom30%S up to a strain of 600%, and for the pom-pom10%S over 90% recovery nearly up to failure.

The most distinct advantage of the pom-pom topology presented here is their outstandingly high UTS via strain hardening, combined with high elongation at break, high Young's modulus, high stress at yield, and in cyclic testing high-stress recovery as well as high maximum stresses. Strain hardening can be attributed to the topology and the phase separation of the rigid PS backbone, which enhances the interdomain connection.

4. CONCLUSIONS

High-performance PS−PI TPEs with a pom-pom topology were investigated, where two stars with PS-*b*-PI arms (with about 13 arms each) are connected by a linear PS chain (M_W = 100 kg mol^{-1}), so PI forms the inner core of the star with 30, 50, 70, and 90 vol % total PI content. Well-defined model systems with narrow polydispersity ($Đ$ < 1.1) were obtained by the following synthetic route: first, a P I-*b*-PS-*b*-PI triblock copolymer (short PI block) was synthesized via anionic polymerization, second, the PI blocks were functionalized via epoxidation and third PS-*b*-PI anions were grafted onto it, within about ∼10 days work for all four samples in the lab. SAXS recommended a cylindrical PI morphology for the pom-pom70%S, a lamellar for the 50%S, a cylindrical PS morphology for the pom-pom30%S, and a spherical PS

morphology for the pom-pom10%S. In mechanical tensile testing, extreme topology-induced strain hardening is found, resulting in very high elongation and stress at break UTS, e.g., for the pom-pom with 70 vol % PI σ_{UTS} = 30 MPa and ε_b = 1200% and with 90% PI σ_{UTS} = 20 MPa and ε_b = 1500%. The UTS benchmark in the literature for PS−PI model systems besides linear SIS triblocks such as stars, miktoarm stars, and MGCs is about σ_{UTS} = 20 MPa, revealing that all the pom-poms can match these values, while the pom-pom30%S outperforms them by nearly 50%. In cyclic tests, 80% stress recovery for the pom-pom50%S, of over 90% for the pom-pom30%S up to a strain of 600%, and for the pom-pom10%S over 90% recovery nearly up to failure were observed. Additionally, for the rubbery pom-pom10%S after cycling loading, small plastic deformation of, e.g., 60% after 1200% of strain remained, which is in the range of the superelastic PS/PI MGC.

For future work, similar directions can be proposed as was done for miktoarm stars, where either PS homopolymers are blended with the branched model systems or common SIS triblock copolymers as a performance-improving additive. Furthermore, the synthesis of pom-pom or barbwire-type materials like MGC with more arms and different $M_{W,a}$ and a PS backbone seems promising.

AUTHOR INFORMATION

Corresponding Author

Valerian Hirschberg − *Institute for Chemical Technology and Polymer Chemistry, Karlsruhe Institute of Technology (KIT), 76131 Karlsruhe, Germany;* orcid.org/0000-0001-8752-930X; Email: valerian.hirschberg@kit.edu

Authors

Max G. Schußmann − *Institute for Chemical Technology and Polymer Chemistry, Karlsruhe Institute of Technology (KIT), 76131 Karlsruhe, Germany*

Marie-Christin Röpert − *Institute for Chemical Technology and Polymer Chemistry, Karlsruhe Institute of Technology (KIT), 76131 Karlsruhe, Germany*

Nico Dingenouts − *Institute for Chemical Technology and Polymer Chemistry, Karlsruhe Institute of Technology (KIT), 76131 Karlsruhe, Germany*

Simon Buchheiser − *Institute of Mechanical Process Engineering and Mechanics, Karlsruhe Institute of Technology (KIT), 76131 Karlsruhe, Germany*

Hermann Nirschl − *Institute of Mechanical Process Engineering and Mechanics, Karlsruhe Institute of Technology (KIT), 76131 Karlsruhe, Germany*

Jonathan Berson − *Institute of Nanotechnology, Karlsruhe Institute of Technology (KIT), 76131 Karlsruhe, Germany;* orcid.org/0000-0002-4979-6359

Manfred Wilhelm − *Institute for Chemical Technology and Polymer Chemistry, Karlsruhe Institute of Technology (KIT), 76131 Karlsruhe, Germany;* orcid.org/0000-0003-2105-6946

Author Contributions

The manuscript was written through contributions of all authors. All authors have given approval to the final version of the manuscript.

Notes

The authors declare no competing financial interest.

ACKNOWLEDGMENTS

The authors thank Dr. Michael Pollard for proofreading as a native English speaker.

REFERENCES

(1) Erman, B.; Mark, J. E.; Roland, C. M. *The Science and Technology of Rubber*, 4th ed.; Academic Press, 2013.

(2) Wang, W.; Lu, W.; Goodwin, A.; Wang, H.; Yin, P.; Kang, N.-G.; Hong, K.; Mays, J. W. Recent advances in thermoplastic elastomers from living polymerizations: macromolecular architectures and supramolecular chemistry. *Prog. Polym. Sci.* **2019**, *95*, 1−31.

(3) Leibler, L. Theory of microphase separation in block copolymers. *Macromolecules* **1980**, *13* (6), 1602−1617.

(4) Fredrickson, G. H.; Helfand, E. Fluctuation effects in the theory of microphase separation in block copolymers. *J. Chem. Phys.* **1987**, *87* (1), 697−705.

(5) Bates, F. S. Polymer-polymer phase behavior. *Science* **1991**, *251* (4996), 898−905.

(6) Heck, M.; Schneider, L.; Müller, M.; Wilhelm, M. Diblock copolymers with similar glass transition temperatures in both blocks for comparing shear orientation processes with DPD computer simulations. *Macromol. Chem. Phys.* **2018**, *219* (9), 1700559.

(7) Khandpur, A. K.; Foerster, S.; Bates, F. S.; Hamley, I. W.; Ryan, A. J.; Bras, W.; Almdal, K.; Mortensen, K. Polyisoprene-polystyrene diblock copolymer phase diagram near the order-disorder transition. *Macromolecules* **1995**, *28* (26), 8796−8806.

(8) Lynd, N. A.; Oyerokun, F. T.; O'Donoghue, D. L.; Handlin, D. L.; Fredrickson, G. H. Design of soft and strong thermoplastic elastomers based on nonlinear block copolymer architectures using self-consistent-field theory. *Macromolecules* **2010**, *43* (7), 3479−3486.

(9) Abu-Sharkh, B.; AlSunaidi, A. Morphology and conformation analysis of self-assembled triblock copolymer melts. *Macromol. Theory Simul.* **2006**, *15* (6), 507−515.

(10) Owens, J. N.; Gancarz, I. S.; Koberstein, J. T.; Russell, T. P. Investigation of the microphase separation transition in low-molecular-weight diblock copolymers. *Macromolecules* **1989**, *22* (8), 3380−3387.

(11) Steube, M.; Johann, T.; Galanos, E.; Appold, M.; Rüttiger, C.; Mezger, M.; Gallei, M.; Müller, A. H. E.; Floudas, G.; Frey, H. Isoprene/styrene tapered multiblock copolymers with up to ten blocks: synthesis, phase behavior, order, and mechanical properties. *Macromolecules* **2018**, *51* (24), 10246−10258.

(12) Heck, M.; Botha, C.; Wilhelm, M.; Hirschberg, V. One-pot synthesis of alternating (ultra-high molecular weight) multiblock copolymers via a combination of anionic polymerization and polycondensation. *Macromol. Rapid Commun.* **2021**, *42* (21), No. e2100448.

(13) Wu, L.; Cochran, E. W.; Lodge, T. P.; Bates, F. S. Consequences of block number on the order−disorder transition and viscoelastic properties of linear $(AB)_n$ multiblock copolymers. *Macromolecules* **2004**, *37* (9), 3360−3368.

(14) Koo, C. M.; Hillmyer, M. A.; Bates, F. S. Structure and properties of semicrystalline-rubbery multiblock copolymers. *Macromolecules* **2006**, *39* (2), 667−677.
(15) Rosenbloom, S. I.; Fors, B. P. Shifting boundaries: controlling molecular weight distribution shape for mechanically enhanced thermoplastic elastomers. *Macromolecules* **2020**, *53* (17), 7479−7486.
(16) Rosenbloom, S. I.; Gentekos, D. T.; Silberstein, M. N.; Fors, B. P. Tailor-made thermoplastic elastomers: customisable materials via modulation of molecular weight distributions. *Chem. Sci.* **2020**, *11* (5), 1361−1367.
(17) Rosenbloom, S. I.; Hsu, J. H.; Fors, B. P. Controlling the shape of the molecular weight distribution for tailored tensile and rheological properties in thermoplastics and thermoplastic elastomers. *J. Polym. Sci.* **2022**, *60* (8), 1291−1299.
(18) Shi, W.; Lynd, N. A.; Montarnal, D.; Luo, Y.; Fredrickson, G. H.; Kramer, E. J.; Ntaras, C.; Avgeropoulos, A.; Hexemer, A. Toward strong thermoplastic elastomers with asymmetric miktoarm block copolymer architectures. *Macromolecules* **2014**, *47* (6), 2037−2043.
(19) Matsen, M. W. Equilibrium behavior of asymmetric ABA triblock copolymer melts. *J. Chem. Phys.* **2000**, *113* (13), 5539−5544.
(20) Beyer, F. L.; Gido, S. P.; Büschl, C.; Iatrou, H.; Uhrig, D.; Mays, J. W.; Chang, M. Y.; Garetz, B. A.; Balsara, N. P.; Tan, N. B.; Hadjichristidis, N. Graft copolymers with regularly spaced, tetrafunctional branch points: morphology and grain structure. *Macromolecules* **2000**, *33* (6), 2039−2048.
(21) Wang, H.; Lu, W.; Wang, W.; Shah, P. N.; Misichronis, K.; Kang, N.-G.; Mays, J. W. Design and synthesis of multigraft copolymer thermoplastic elastomers: superelastomers. *Macromol. Chem. Phys.* **2018**, *219* (1), 1700254.
(22) Uhrig, D.; Mays, J. W. Synthesis of combs, centipedes, and barbwires: poly(isoprene-graft-styrene) regular multigraft copolymers with trifunctional, tetrafunctional, and hexafunctional branch points. *Macromolecules* **2002**, *35* (19), 7182−7190.
(23) Weidisch, R.; Gido, S. P.; Uhrig, D.; Iatrou, H.; Mays, J.; Hadjichristidis, N. Tetrafunctional multigraft copolymers as novel thermoplastic elastomers. *Macromolecules* **2001**, *34* (18), 6333−6337.
(24) Zhu, Y.; Burgaz, E.; Gido, S. P.; Staudinger, U.; Weidisch, R.; Uhrig, D.; Mays, J. W. Morphology and tensile properties of multigraft copolymers with regularly spaced tri-tetra-and hexafunctional junction points. *Macromolecules* **2006**, *39* (13), 4428−4436.
(25) Schlegel, R.; Duan, Y. X.; Weidisch, R.; Hölzer, S.; Schneider, K.; Stamm, M.; Uhrig, D.; Mays, J. W.; Heinrich, G.; Hadjichristidis, N. High-strain-induced deformation mechanisms in block-graft and multigraft copolymers. *Macromolecules* **2011**, *44* (23), 9374−9383.
(26) Lequieu, J.; Koeper, T.; Delaney, K. T.; Fredrickson, G. H. Extreme deflection of phase boundaries and chain bridging in $A(BA')_n$ miktoarm star polymers. *Macromolecules* **2020**, *53* (2), 513−522.
(27) Shi, W.; Fredrickson, G. H.; Kramer, E. J.; Ntaras, C.; Avgeropoulos, A.; Demassieux, Q.; Creton, C. Mechanics of an asymmetric hard-soft lamellar nanomaterial. *ACS Nano* **2016**, *10* (2), 2054−2062.
(28) Shi, W.; Hamilton, A. L.; Delaney, K. T.; Fredrickson, G. H.; Kramer, E. J.; Ntaras, C.; Avgeropoulos, A.; Lynd, N. A. Creating extremely asymmetric lamellar structures via fluctuation-assisted unbinding of miktoarm star block copolymer alloys. *J. Am. Chem. Soc.* **2015**, *137* (19), 6160−6163.
(29) Knoll, K.; Nieβner, N. Styroflex: a new transparent styrene-butadiene copolymer with high flexibility. In *Applications of Anionic Polymerization Research*; Quirk, R. P., Ed.; *ACS Symposium Series*; American Chemical Society, 1998; pp 112−128..
(30) Knoll, K.; Nießner, N. Styrolux$^+$ and styroflex$^+$—from transparent high impact polystyrene to new thermoplastic elastomers: syntheses, applications and blends with other styrene based polymers. *Macromol. Symp.* **1998**, *132* (1), 231−243.
(31) von Tiedemann, P.; Yan, J.; Barent, R. D.; Spontak, R. J.; Floudas, G.; Frey, H.; Register, R. A. Tapered multiblock star copolymers: synthesis, selective hydrogenation, and properties. *Macromolecules* **2020**, *53* (11), 4422−4434.
(32) Bi, L.-K.; Fetters, L. J. Domain morphology of star block copolymers of polystyrene and polyisoprene. *Macromolecules* **1975**, *8* (1), 90−92.
(33) Bi, L.-K.; Fetters, L. J. Synthesis and properties of block copolymers. 3. Polystyrene-polydiene star block copolymers. *Macromolecules* **1976**, *9* (5), 732−742.
(34) Hutchings, L. R.; Agostini, S.; Hamley, I. W.; Hermida-Merino, D. Chain architecture as an orthogonal parameter to influence block copolymer morphology. synthesis and characterization of hyperbranched block copolymers: hyperblocks. *Macromolecules* **2015**, *48* (24), 8806−8822.
(35) Hutchings, L. R.; Dodds, J. M.; Roberts-Bleming, S. J. HyperMacs: highly branched polymers prepared by the polycondensation of AB_2 macromonomers, synthesis and characterization. *Macromolecules* **2005**, *38* (14), 5970−5980.
(36) Hutchings, L. R.; Dodds, J. M.; Rees, D.; Kimani, S. M.; Wu, J. J.; Smith, E. HyperMacs to HyperBlocks: a novel class of branched thermoplastic elastomer. *Macromolecules* **2009**, *42* (22), 8675−8687.
(37) Jiang, F.; Wang, Z.; Qiao, Y.; Wang, Z.; Tang, C. A novel architecture toward third-generation thermoplastic elastomers by a grafting strategy. *Macromolecules* **2013**, *46* (12), 4772−4780.
(38) Polymeropoulos, G.; Zapsas, G.; Ntetsikas, K.; Bilalis, P.; Gnanou, Y.; Hadjichristidis, N. 50th Anniversary perspective: polymers with complex architectures. *Macromolecules* **2017**, *50* (4), 1253−1290.
(39) Hadjichristidis, N. Synthesis of miktoarm star (?-star) polymers. *J. Polym. Sci., Part A: Polym. Chem.* **1999**, *37* (7), 857−871.
(40) Liontos, G.; Manesi, G.-M.; Moutsios, I.; Moschovas, D.; Piryazev, A. A.; Bersenev, E. A.; Ivanov, D. A.; Avgeropoulos, A. Synthesis, molecular characterization, and phase behavior of miktoarm star copolymers of the AB_n and A_nB (n = 2 or 3) sequences, where A is polystyrene and B is poly(dimethylsiloxane). *Macromolecules* **2022**, *55* (1), 88−99.
(41) Ward, I. I.; Sweeney, J. *Mechanical Properties of Solid Polymers*, 3rd ed.; John Wiley & Sons, 2012.
(42) Röpert, M. C.; Schußmann, M. G.; Esfahani, M. K.; Wilhelm, M.; Hirschberg, V. Effect of side chain length in polystyrene POM-POMs on melt rheology and solid mechanical fatigue. *Macromolecules* **2022**, *55*, 5485−5496.
(43) Röpert, M.; Goecke, A.; Wilhelm, M.; Hirschberg, V. Threading polystyrene stars: impact of star to POM-POM and barbwire topology on melt rheological and foaming properties. *Macromol. Chem. Phys.* **2022**, *223*, 2200288.
(44) Yuan, Z.; Gauthier, M. Synthesis of arborescent isoprene homopolymers. *Macromolecules* **2005**, *38* (10), 4124−4132.
(45) Hirschberg, V.; Faust, L.; Rodrigue, D.; Wilhelm, M. Effect of topology and molecular properties on the rheology and fatigue behavior of solid polystyrene/polyisoprene di- and triblock copolymers. *Macromolecules* **2020**, *53* (13), 5572−5587.
(46) Hamley, I. W. *The Physics of Block Copolymers*; Oxford Science Publications; Oxford University Press, 2003.
(47) Ishizu, K.; Uchida, S. Synthesis and microphase-separated structures of star-block copolymers. *Prog. Polym. Sci.* **1999**, *24* (10), 1439−1480.